Geological Magazine

www.cambridge.org/geo

Crust–mantle interactions in Zijinshan ore field identified by zircon SIMS U–Pb age and zircon Hf–O isotopes

Wen-Hui Zhang, Shuai-Qi Yan and Li-Yuan Wang

Zijin School of Geology and Mining, Fuzhou University, Fuzhou 350108, China

Original Article

Cite this article: Zhang W-H, Yan S-Q, and Wang L-Y (2023) Crust–mantle interactions in Zijinshan ore field identified by zircon SIMS U–Pb age and zircon Hf–O isotopes. *Geological Magazine* **160**: 292–304. https://doi.org/10.1017/S0016756822000863

Received: 30 August 2021
Revised: 19 July 2022
Accepted: 23 July 2022
First published online: 26 September 2022

Keywords:
SIMS zircon U–Pb age; Hf–O isotopes; crust-mantle interactions; Zijinshan ore field; granite

Author for correspondence:
Wang Li-yuan,
Email: wangliyuan030101@163.com

Abstract

This study presents zircon U–Pb geochronology and Hf and O isotope data for granitic rocks in the Zijinshan ore field, southwestern Fujian Province, China. The intrusive rocks comprise monzogranite, granite and granodiorite. The magmatic zircon U–Pb ages from these granitic rocks can be divided into four episodes: episodes 1 (157.9–159.9 Ma) and 2 (141 Ma) in the Late Jurassic and episodes 3 (108.1–103.2 Ma) and 4 (97.5–99.7 Ma) in the Middle and Late Cretaceous, respectively. Patterns of rare-earth elements (REE) show enrichment in light REE and obvious negative Eu anomalies. These rocks are also enriched in Rb, Th, U, La, Ce, Nd and Hf, and depleted in Ba, Nb, Sr, P and Ti. The increasing La/Yb ratio and decreasing heavy REE content with decreasing age may imply an increasing contribution of mantle-derived materials from the Late Jurassic to Cretaceous. The zircon $\epsilon_{Hf}(t)$ and $\delta^{18}O$ values, ranging from −37.7 to −2.8 and 12.0 ‰ to 6.3 ‰, respectively, indicate that the lower crust is an important source of granitic rocks. There was a significant increase in $\epsilon_{Hf}(t)$ values and a decrease in $\delta^{18}O$ values in the younger magmatic episodes (3 and 4), which ranged from −11.4 to −0.6 and 10.7 to 6.3 ‰, respectively. This suggests an increasing contribution of mantle-derived magma to the crustal melts from the Late Jurassic to late Early Cretaceous in response to the changing regional tectonic setting from compression to extension and an increasing interaction between the crust and mantle.

1. Introduction

The Zijinshan area is located in southwestern Fujian Province, China (Fig. 1). As almost all the magmatic rocks in the Zijinshan area experienced intense alteration, attention has been focused on magmatic zircon studies. Previous studies on zircon U–Pb ages (Jiang *et al.* 2013, 2015; Liang *et al.* 2013; Yu *et al.* 2013;; Xu *et al.* 2017) have shown that the Mesozoic magmatic rocks in this area mainly include intrusive rocks from the Middle Jurassic and intrusive-volcanic rocks from the Early Cretaceous. This large-scale Late Mesozoic magmatic activity is closely related to the formation of Cu, Au, Fe, Pb, Zn and Ag mineral deposits (Chen, 1999; Zhang *et al.* 2001; Mao *et al.* 2006; Liang *et al.* 2013; Jiang *et al.* 2015; Li *et al.* 2015; Duan *et al.* 2017; Xu *et al.* 2017). The petrogenesis and magmatic evolution processes of the Zijinshan area Mesozoic magmatic rocks are still a topic of debate, with the contribution of mantle material being unclear. Wang *et al.* (2005) and He *et al.* (2010) suggested that the Indosinian subcontinent mantle in the South China area was an enriched mantle (EM II); most zircon $\epsilon_{Hf}(t)$ values are lower than depleted mantle values, which indicates an enriched source for many granitic rocks on the southeast coast (Li *et al.* 2014). An increasing $\epsilon_{Hf}(t)$ trend in the SE China Mesozoic magmas implies an increasing impact from a depleted asthenospheric mantle over time from the Late Jurassic to the Late Cretaceous. These rocks were derived from the mixing of different proportions of mantle-derived components with Palaeoproterozoic basement crust-derived magmas (He & Xu, 2012; Liu *et al.* 2014).

The Zijinshan granitic complex (164–155 Ma) exhibits negative whole-rock $\epsilon_{Nd}(t)$ values (−10.3 to −6.8) and $\epsilon_{Hf}(t)$ values (−19.0 to −7.1), which, together with geochemical data, suggest that the Zijinshan granitic complex was most likely derived from the mixing of juvenile components and partial melting of the crust materials including Proterozoic orthometamorphic and parametamorphic rocks (Li *et al.* 2015). Studies of Cretaceous magmatic rocks in the Zijinshan mineral field reveal arc-like geochemical signatures, with the heterogeneous Hf isotopic compositions ($\epsilon_{Hf}(t)$ range of −9.4 to +0.1) of zircons suggesting an origin from mixing between crustal- and subduction-related mantle-derived melts due to lithospheric extension in response to subduction of the Pacific plate (Jiang *et al.* 2013; Wang *et al.* 2013; Li *et al.* 2015; Chi *et al.* 2020). Muscovite ^{40}Ar–^{39}Ar and molybdenite Re–Os ages (113–105 Ma) for mineralization are coeval with the ages of the late Early Cretaceous rocks (Duan *et al.* 2017; Huang *et al.* 2018; Zhao *et al.* 2020). The zircons in late Early Cretaceous rocks have elevated Ce^{4+}/Ce^{3+} values, indicating high oxygen fugacity. This suggests that the rocks formed from the mixing of

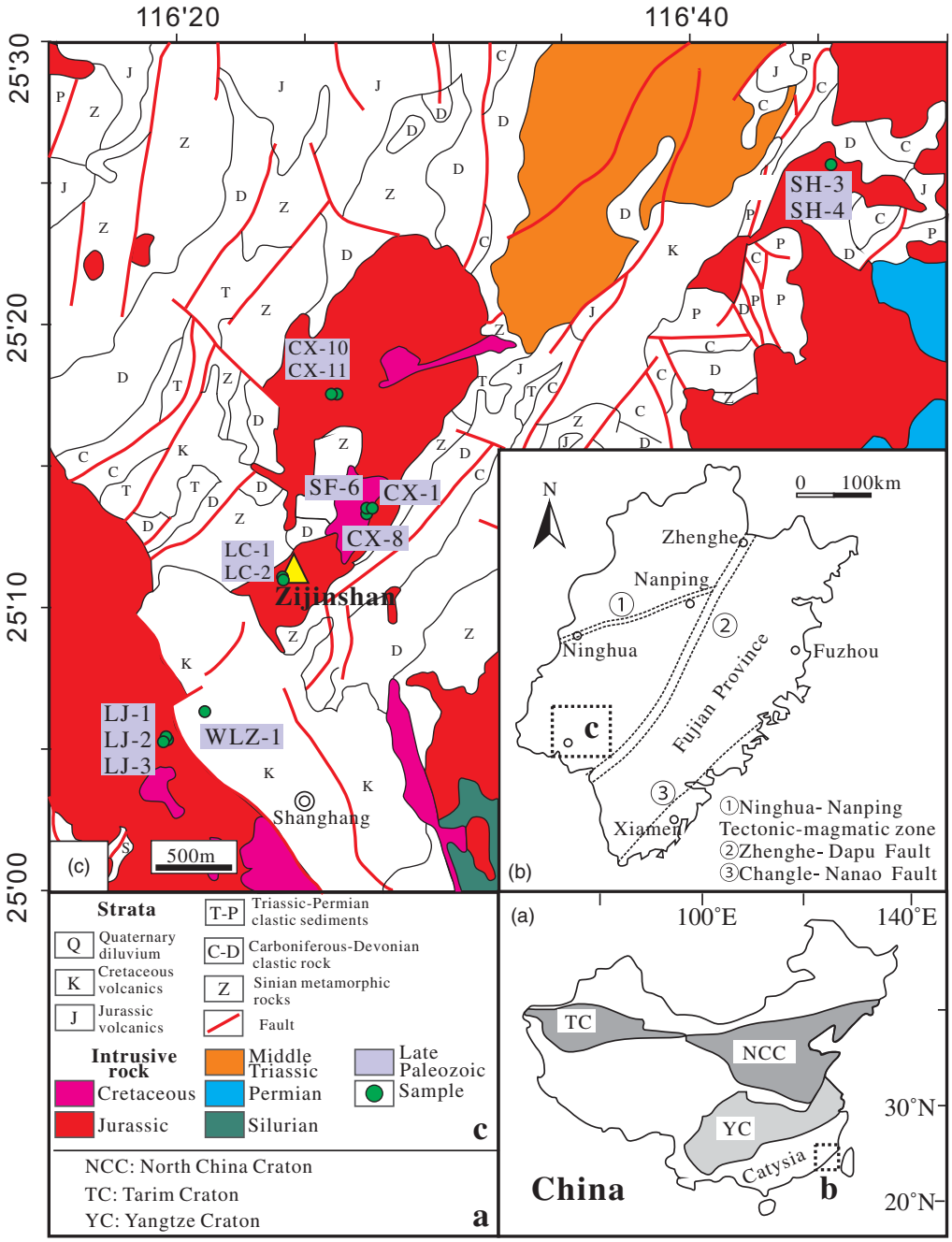

Fig. 1. (Colour online) Geological sketch map of China (a), Fujian Province (b) and Zijinshan area (c).

subduction-related metasomatized mantle-derived high fO_2 melts with crustal melts, whereas the Middle to Late Jurassic rocks were derived from the partial melting of crustal materials. This implies that the early Late Cretaceous rocks are characterized by higher oxygen fugacity with higher mineralization potential than the Middle to Late Jurassic rocks (Zhong *et al.* 2014; Duan *et al.* 2017; Chi *et al.* 2020).

Magmatic zircon is an ideal mineral for age determination and petrogenesis studies of granitic rocks because of its high closure temperature for Pb and Hf, high U/Pb ratios and low Lu/Hf ratios. Owing to the development of *in situ* isotope analysis technology, isotope signatures of zircons with different ages and compositions can be used to reveal the genesis and evolutionary process of granitic rocks (Wu *et al.* 2007). The presence of a large number of magmatic zircons in granites provides a clue to the magmatic history and the evolution of the magmatic source, and whether they experienced intense alteration. Concurrently, the O isotopes of magmatic zircon grains in equilibrium with mantle-derived magmas show a well-constrained and narrow range of $\delta^{18}O$ values (*c.* 5.3 ± 0.3 ‰). This mantle zircon value is insensitive to magmatic differentiation, because the increase in bulk rock $\delta^{18}O$ value is compensated for by an increase in zircon/liquid $\delta^{18}O$ fractionation. Magmatic zircons derived from low- and high-temperature hydrothermally altered sources should have distinct O isotope compositions (Chen *et al.* 2003; Valley *et al.* 2005). Therefore, zircon O isotope analysis is effective in tracing the involvement of crustal and mantle materials in the magmatic source and in providing robust constraints on crust–mantle interactions and the contribution of mantle-derived materials to the formation of granites (Li *et al.* 2009*a*). Preliminary studies on the zircon O isotope

https://doi.org/10.1017/S0016756822000863 Published online by Cambridge University Press

characteristics of the host magmatic rocks show the Early Palaeozoic, Late Triassic and Late Jurassic magmatic rocks were mainly sourced from the crust (Zhang *et al.* 2017).

Because young (<200 Ma) juvenile crustal rocks will still have similar Hf isotopic composition to that of the depleted mantle, Hf isotope composition alone cannot effectively distinguish between mantle-derived and the young juvenile crustal-derived magmas involved in granite formation (Li *et al.* 2009a; Morag *et al.* 2011). Therefore, a combined study of zircon Hf and O isotopes could play an important role in exploring the characteristics and relative importance of the potential mantle and crustal sources and magmatic evolution.

In this study, we present *in situ* data for zircon U, Pb, O and Hf isotope compositions, as well as whole-rock major and trace elements for the Mesozoic granitic rocks in the Zijinshan area. This data allowed discrimination between the new and reworked crust and helped us understand the magmatic evolution of the Zijinshan ore field.

2. Geological background and petrography

2.a. Geological background

The study area is located in the southwest depression zone of Fujian, and west of the NW-striking Zhenghe–Dapu deep fault zone, which extends for more than 1000 km (Fig. 1b). The NW-striking Yunxiao–Shanghang fault zone and NE-orienting Xuanhe zone anticlines intersect in the Zijinshan area. The Indosinian orogeny occurred in eastern China during the Early Triassic period. The tectonic framework changed from the predominant Tethys tectonic domain to the Circum-Pacific active continental margin, with intense tectonic deformation, magmatism and related mineralization, forming a series of granitoid belts (Mao *et al.* 2001). The outcropped basement strata in the Zijinshan area are Late Neoproterozoic and Early Palaeozoic low-grade metamorphic rocks of flysch sediments. Late Jurassic and Early Cretaceous granitoids are widely distributed in this region (Fig. 1). Secondary ion mass spectrometry (SIMS) U–Pb ages of magmatic zircons from Mesozoic granitoids and mafic dikes show five separate episodes of magmatism (Zhang *et al.* 2017): Early Proterozoic, Middle–Late Proterozoic, Silurian – Late Triassic, Late Jurassic and Early Cretaceous. Mesozoic Zijinshan magmatism occurred in two major phases: (1) Middle to Late Jurassic Zijinshan granitoids and (2) Early Cretaceous Shimaoshan volcanic rocks, Sifang granodiorite, porphyritic granodiorite and late aplite dykes (Xu *et al.* 2017).

2.b. Petrography

Thirteen granitic rocks were sampled from the Zijinshan plutons. These samples were mainly composed of monzogranite and granodiorite (Table 1). The monzogranite samples (CX-1, CX-8, LC-2, SH-3, SH-4, LJ-1, LJ-2, LJ-3, SF-6 and WLZ-1) were pink in colour, medium- to coarse-grained (Fig. 2a) and massive-structured. The monzogranite comprises quartz (25–35 %), plagioclase (25–30 %), alkaline feldspar (30–35 %), biotite (<5 %) and hornblende (1–3 %). The plagioclase occurred as euhedral to subhedral tabular crystals with polysynthetic albite twinning, exhibiting normal and oscillatory zoning. The grain size of the alkali feldspar was 2–5 mm, containing mainly orthoclase and perthite with evident Carlsbad twins (Fig. 2b) and perthitic texture (Fig. 2c), respectively. The quartz was inlaid in xenomorphic grains, and sericitization was common on the surface of the plagioclase (Fig. 2a–c) with polycrystalline twins and rhythmic bands (Fig. 2e). The biotite was often chloritized and the alkaline feldspar was often kaolinized.

The granodiorites (CX-10, CX-11) were light grey in colour, medium- to fine-grained (Fig. 2g) and composed of plagioclase (50%–55 %), K-feldspar (20%–25 %), quartz (20%–25 %), biotite (5%–10 %) and hornblende (1%–3 %), along with accessory magnetite, titanite, zircon and allanite. The plagioclase grains were usually polycrystalline twinned crystals of 2–3 mm; the potassium feldspar was light flesh red and occurred as euhedral to subhedral phenocrysts, with a size of 2–4 mm. Kaolinization of K-feldspar was commonly observed. Chloritization often occurred in the hornblende and biotite (Fig. 2h) while sericitization occurred in the plagioclase (Fig. 2i). One sample (LC-1) was mainly composed of quartz because of strong silicification. The protolith was a quartz porphyry, which developed into siliceous rock under the action of later fluid.

3. Analytical methods

3.a. Major and trace element analysis

Thirteen samples were collected for major and trace element study of whole rocks. These samples were crushed and ground to 200-mesh using an agate ring mill. The major and trace elements were analysed at the Institute of Regional Geology and Mineral Resources Survey in Hebei Province, China. Samples for major element analysis were fused into glass discs and analysed with X-ray fluorescence spectroscopy (XRF) using an AXIOS Minerals Spectrometer. Precision for the analytical results was typically 1–5 %. Rare-earth and other trace elements were analysed using inductively coupled plasma mass spectroscopy (ICP-MS) at the same institute. The whole-rock powders (50 mg) were dissolved in high-pressure Teflon bombs using an HF + HNO_3 mixture for 48 h at ~200 °C. The analytical uncertainties for most trace elements were generally better than 5 %, monitored by analyses of Chinese national standard samples GSR-1 and GSR-3.

3.b. Oxygen isotope analysis

Zircon *in situ* O isotopes were also analysed at the Institute of Geology and Geophysics using the Cameca IMS 1280 ion microprobe (CASIMS). The detailed analysis method can be found in Li *et al.* (2012). A single $^{133}Cs^{+}$ ion beam with 2nA strength bombed the sample surface, and received both ^{16}O and ^{18}O simultaneously with two Faraday cups. The single-point measurement time was *c.* 5 min, the accuracy of the single group $^{18}O/^{16}O$ data is generally better than 0.2–0.3 ‰ (1σ), and the external precision of the sample was 0.5 ‰ (2SD). The reference material used for calibration of instrumental mass fractionation (IMF) was the Penglai zircon standard (Li *et al.* 2010), which was mounted together with the samples. The measured $^{18}O/^{16}O$ ratio was corrected with the Vienna Standard Mean Ocean Water (V-SMOW) value ($^{18}O/^{16}O = 0.0020052$). In this study: $(\delta^{18}O)_M = [(^{18}O/^{16}O)_M/0.0020052 - 1) \times 1000(‰]$, $IMF = (\delta^{18}O)_{M(standard)} - (\delta^{18}O)_{V\text{-}SMOW}$, $\delta^{18}O_{sample} = (\delta^{18}O)_M + IMF$.

3.c. Zircon U–Pb dating

Eight samples were selected for zircon U–Pb, Hf and O isotope analysis. Zircons from *c.* 20 kg of the sample were first separated using magnetic and heavy liquid separation methods in order to concentrate them, and then hand-picked under a binocular microscope. Generally, more than 1000 grains of zircon were extracted

https://doi.org/10.1017/S0016756822000863 Published online by Cambridge University Press

Table 1. Rock sample information

Sample ID	Coordinates	Rock type	Phase	U–Pb age (Ma)	Zircon $\delta^{18}O$ range (‰)		Mean zircon $\delta^{18}O$	Mean $\varepsilon_{Hf}(t)$	$\varepsilon_{Hf}(t)$ range
CX-1	25° 13′ 22.8″ N, 116° 27′ 45.9″ E	Monzogranite	Episode 1	159.9 ± 1.3	6.49–8.84	6.49–11.96	8.18	−11.3	0.7 to −37.7
SH-3	25° 25′ 45.3″ N, 116° 45′ 41.3″ E	Monzogranite	Episode 1	158.4 ± 1.3	7.41–9.14		8.01	−7.5	
LC-1	25° 11′ 05.7″ N, 116° 24′ 07.7″ E	Quartz porphyry	Episode 1	157.9 ± 2.0	5.51–10.55		8.3	−8.1	
LC-2	25° 11′ 18.5″ N, 116° 24′22.6″ E	Monzogranite	Episode 1		7.8–11.96		8.6	−11	
CX-10	25° 16′ 29.0″ N, 116° 25′ 24.9″ E	Granodiorites	Episode 2		7.58–8.59	7.41–8.59	8.04	−11.7	
CX-11	25° 17′ 26.6″ N, 116° 26′ 10.2″ E	Monzogranite	Episode 2	141.0 ± 1.2	7.18–8.29		7.84	−10.4	−22.6 to −7.3
CX-8	25° 13′ 12.4″ N,116° 27′ 28.8″ E	Monzogranite	Episode 3	108.1 ± 0.81	6.29–7.24	6.28–7.78	6.78	−2.3	−0.6 to −11.2
LJ-1	25° 06′ 18.9″ N, 116° 19′ 38.4″ E	Monzogranite	Episode 3	103.2 ± 0.60	6.28–7.78		6.87	−6.3	
SF-6	25° 13′ 12.4″ N, 116° 27′ 28.8″ E	Monzogranite	Episode 4	99.42 ± 0.47	6.84–10.73	6.64–8.56	7.82	−6.7	−2.8 to −11.4
WLZ-1	25° 06′ 51.3″ N, 116° 20′ 13.4″ E	Monzogranite	Episode 4	97.53 ± 0.87	5.5–7.6		7.07	−6.5	

from each sample. Zircon grains and zircon standard samples (Qinghu, Plésovice and 91500) were mounted in epoxy resin, polished to expose the interior of the grains and then coated with gold. The morphology and internal structure of the zircons were studied using the cathodoluminescence (CL) technique, using a JXA-8100 Electron Probe Microanalyzer for high-resolution imaging and energy-dispersive X-ray spectroscopy (EDS) at the State Key Laboratory of Continental Tectonics and Dynamics, Chinese Academy of Geological Sciences. The *in situ* O isotope ratios were analysed first and then the U–Pb data and Hf isotope analyses were repeated at the same sites previously analysed.

Zircon U–Pb dating was conducted using the CASIMS at the Institute of Geology and Geophysics, Chinese Academy of Sciences (IGGCAS), in Beijing. The detailed analytical method can be found in Li *et al.* (2009b). Analyses were carried out with a beam diameter of 36 μm, 5 Hz repetition rate and energy of 10–20 J cm^{-2}. A single O^{2-} ion beam (20 μm × 30 μm in size and strength of 10 nA) bombarded the sample surface with an acceleration voltage of −13 kV. Oxygen flow was used to increase the sample chamber pressure to *c.* 5×10^{-6} T in order to improve the sensitivity to the Pb^{+} ion in zircon. Seven sets of data were analysed for each sample spot and the measuring time was *c.* 12 min. Internal zircon standards prototype Plésovice and Qinghu (Li *et al.* 2013) were measured alternately. The obtained standard deviation of 1.5 % (1σ) of the long-term monitoring standard sample (Li *et al.* 2010) and the internal test accuracy of a single sample point together determine the single point error. The zircon 91500 standard (1065 Ma) was used as an external standard to correct Pb/U ratios and calculate Th and U content of zircon samples (Th = 29 μg g^{-1}; U = 81 μg g^{-1}) (Wiedenbeck *et al.* 1995). The common Pb correction for the measured compositions was based on non-radiogenic ^{204}Pb. The uncertainties given in the tables in the Supplementary Material available online at https://doi.org/10.1017/S0016756822000863 were 1σ for individual isotopic analyses.

3.d. Hf isotope analysis

Lu–Hf isotope analyses were conducted on the same zircon grains that were previously analysed for O isotope compositions and U–Pb geochronology. *In situ* zircon Lu–Hf isotope measurements were performed using a Neptune Plus MC-ICP-MS, coupled with a Resolution 193 nm laser ablation system at the Institute of Geology and Geophysics. This instrument is a double focusing multi-collector ICP-MS and can take high-mass-resolution measurements in multiple collector modes. A detailed description of analytical methods can be found in Wu *et al.* (2006). The laser ablation time was 26 s. The laser ablation pulse frequency was 10 Hz and the pulse power was 100 mJ, with a beam spot size of *c.* 60 μm. Isobaric interference of ^{176}Lu and ^{176}Yb to ^{176}Hf was rectified by monitoring ^{175}Lu and ^{172}Yb signal strength, using the $^{175}Lu/^{176}Lu$ ratio (0.02655) and $^{176}Yb/^{172}Yb$ ratios (0.5886) (Chu *et al.* 2002). Zircon standard 91500 cross-referenced with zircon sample analysis was used for external monitoring of the instrument drift. In the process of analysis, the average $^{176}Hf/^{177}Hf$ ratio for the zircon standard Mud Tank was 0.282491 ± 27 (2σ), and for GJ it was 0.281971 ± 26 (2σ), which is consistent with the error range reported in the literature (Geng *et al.* 2011; Li *et al.* 2013). The ϵ_{Hf} value and two-stage depleted mantle model ages were calculated according to Wu *et al.* (2007) and references therein, using $(^{176}Lu/^{177}Hf)_{CHUR} = 0.0332$; $(^{176}Hf/^{177}Hf)_{CHUR,0} = 0.28277$; $(^{176}Lu/^{177}Hf)_{DM} = 0.0384$; $(^{176}Hf/^{177}Hf)_{DM} = 0.28325$.

4. Results

4.a. Zircon SIMS U–Pb ages

The zircons in this study were mostly colourless and transparent crystals, semi-automorphic to idiomorphic, with a length of 100–400 μm and a length-to-width ratio of 1:1 to 4:1. Cathodoluminescence images showed that the internal structure of the zircons exhibited clear oscillating zoning (Fig. 3). No

https://doi.org/10.1017/S0016756822000863 Published online by Cambridge University Press

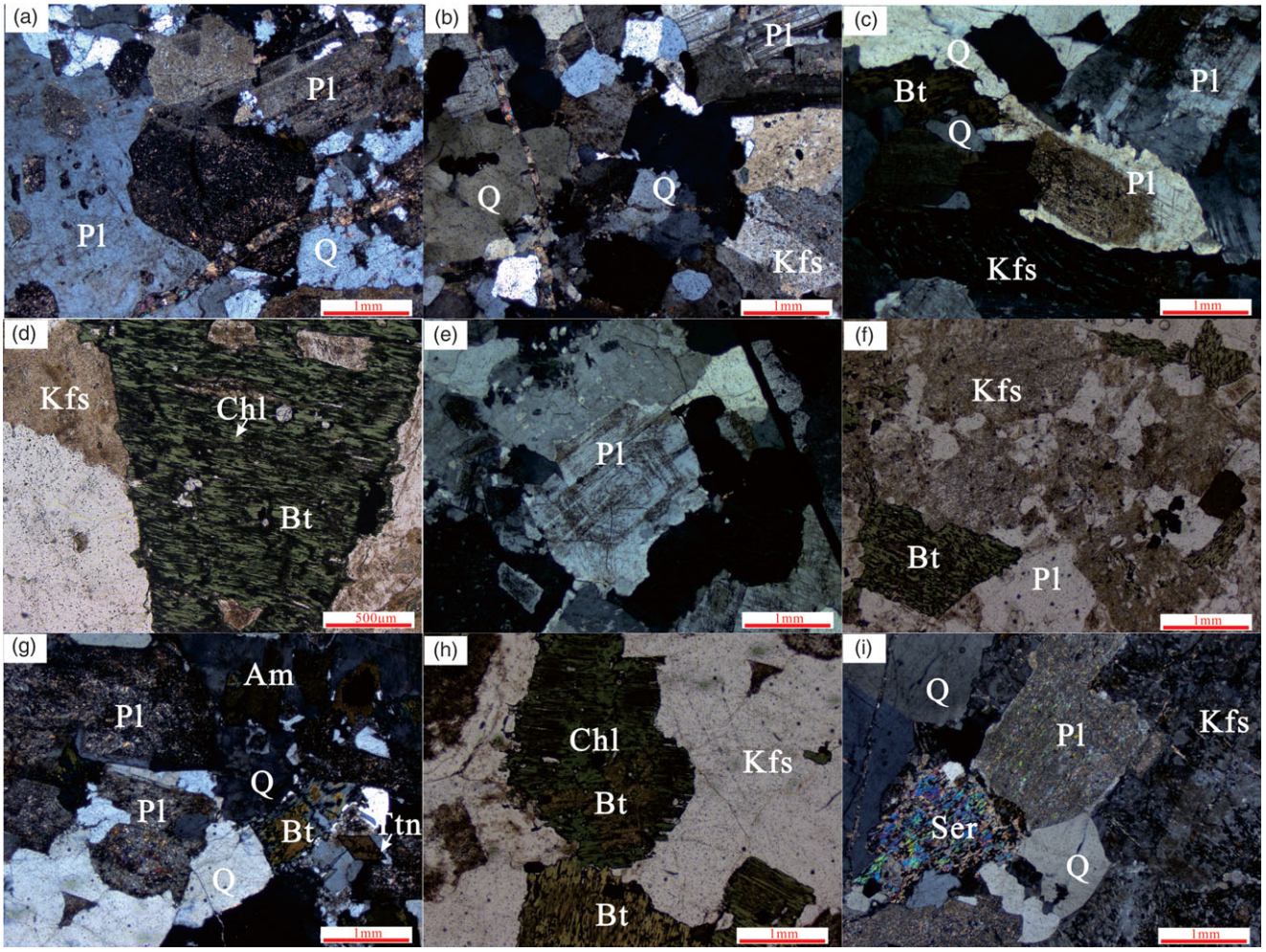

Fig. 2. (Colour online) Thin-section photomicrographs of monzonitic granite (a–f) and granodiorite (g–i) in the Zijingshan area. (a) Plagioclase sericization; (b, c) granitic structure, plagioclase polycrystalline and potassium feldspar caspar twin and perthitic texture are developed; (d) chloritization often occurs in biotite; (e) plagioclase crystals show complex oscillatory zoning with resorption surfaces; (f) potassium feldspar clay mineralization development; (g) plagioclase in granodiorite sericitization; (h) biotite in granodiorite altered to chlorite; (i) most plagioclase is completely altered into sericite. Q – quartz; Pl – plagioclase; Per – perthite; Am – amphibole; Bt – biotite; Ttn – titanite; Ser – sericite.

influence of the alteration on these zircon grains was observed. The Th/U ratios of the zircons were generally >0.1 (Supplementary Table A.1 in the Supplementary Material available online at https://doi.org/10.1017/S0016756822000863), which is typical of magmatic zircons (Belousova *et al.* 2002). The detailed dating results are listed in online Supplementary Table A.2. We use the $^{206}Pb/^{238}U$ age in the following discussion because it is more precise for younger zircons (Griffin *et al.* 2004).

Samples CX-1, SH-3 and LC-1 displayed the oldest ages, in the range 157.9–159.9 Ma. Thirteen analyses from sample CX-1 yielded concordant $^{206}Pb/^{238}U$ ages ranging from 156.5 ± 2.4 to 163.5 ± 2.4 Ma, with a weighted mean age of 159.9 ± 1.3 Ma (MSWD = 1.9; Supplementary Table A.2; Fig. 4). Fifteen analyses from sample SH-3 yielded concordant $^{206}Pb/^{238}U$ ages ranging from 157.0 ± 2.4 to 161.2 ± 2.4 Ma, with a weighted mean age of 158.4 ± 1.3 Ma (MSWD = 0.25), excluding one younger age of 145.7 ± 2.2 Ma. Eleven analyses from sample LC-1 yielded concordant $^{206}Pb/^{238}U$ ages between 149.0 ± 2.2 and 162.8 ± 2.4 Ma, with a weighted mean age of 157.9 ± 2.0 Ma (MSWD = 4.9). Spots -9, 5 and 13 yielded much older $^{206}Pb/^{238}U$ ages of 933.3 ± 15.2 Ma, 257.2 ± 3.8 Ma and 229.2 ± 3.4 Ma, respectively, interpreted as the ages of xenocrystic zircons in the early intrusive or volcanic rocks.

Thirteen analyses from sample CX-11 yielded concordant $^{206}Pb/^{238}U$ ages ranging from 138.7 ± 2.1 to 143.5 ± 2.1 Ma, with a weighted mean age of 141.0 ± 1.2 Ma (MSWD = 3.0; Fig. 4). One spot (9) from sample CX-11 yielded an age of 704.7 ± 10.0 Ma. Sixteen analyses from sample CX-8 yielded concordant $^{206}Pb/^{238}U$ ages ranging from 104.6 ± 0.9 to 112.6 ± 2.2 Ma, with a weighted mean age of 108.1 ± 0.81 Ma (MSWD = 4.4; Fig. 4). Fourteen analyses from Sample LJ-1 yielded concordant $^{206}Pb/^{238}U$ ages ranging from 113.9 ± 3.5 to 92.3 ± 2.2 Ma, with a weighted mean age of 103.2 ± 0.60 Ma (MSWD = 1.03). Spot 13 had a much lower $^{206}Pb/^{238}U$ age of 69.1 ± 1.7 Ma, likely due to the loss of lead.

Eleven analyses from sample SF-6 yielded concordant $^{206}Pb/^{238}U$ ages between 97.5 ± 1.5 and 101.1 ± 1.5 Ma, with a weighted mean age of 99.42 ± 0.47 Ma (MSWD = 0.84). Spots 2, 4, 12 and 13 had higher $^{206}Pb/^{238}U$ ages ranging from 220.4 ± 3.3 to 226.4 ± 3.4 Ma, which was interpreted as xenocrystic zircon. Thirteen analyses from sample WLZ-1 yielded concordant

https://doi.org/10.1017/S0016756822000863 Published online by Cambridge University Press

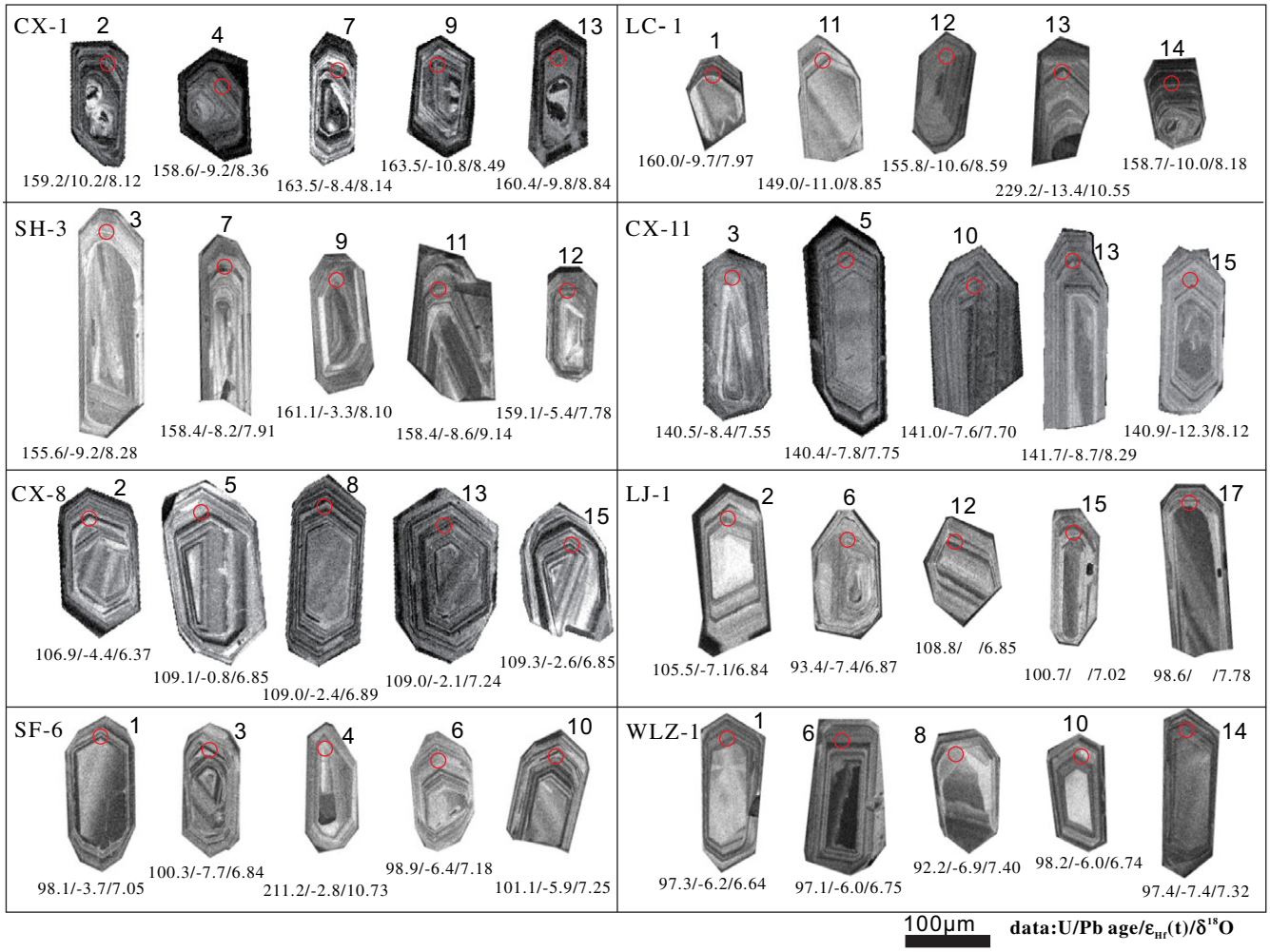

Fig. 3. (Colour online) Zircon cathodoluminescence images. Red circles represent the analysis location of Hf–O and U–Pb isotopes in the CL image. Small red numbers indicate U–Pb dating ages; white numbers indicate Lu–Hf isotope $\epsilon_{Hf}(t)$ values; yellow numbers indicate zircon $\delta^{18}O$ values.

$^{206}Pb/^{238}U$ ages ranging from 92.2 ± 1.5 to 99.2 ± 1.5 Ma, with a weighted mean age of 97.53 ± 0.87 Ma (MSWD = 1.3). Overall, the average samples age can be divided into four episodes: 157.9–159.9 (samples CX-1, SH-3, LC-1), 141 (CX-11), 108.1–103.2 (CX-8, LJ-1) and 97.5–99.7 Ma (SF-6, WLZ-1), respectively.

4.b. Characteristics of major and trace elements

Thirteen samples were analysed for major and trace element compositions (Supplementary Table A.1, available online at https://doi.org/10.1017/S0016756822000863). The whole-rock SiO_2 contents of the samples were mainly in the range 65.57–77.54 wt %. (Fig. 5). Zircon U–Pb age and microscopic features suggest that granitic rocks were intruded during the 157.9–159.9 Ma episode, which mainly consisted of granite; those intruded in the 141 Ma and the 108.1–103.2 Ma episodes consisted of granodiorite and quartz monzonite, and those in the 97.5–99.7 Ma episode consisted only of granite. Relatively higher SiO_2 content is usually associated with lower contents of $Fe_2O_3^T$, MgO and CaO.

LC-1 and LC-2 are much more depleted of rare-earth elements (REE) and also show a trend of heavier REE (HREE) enrichment. Most of the samples show similar chondrite-normalized REE patterns (Fig. 6a): enrichment in light REE (LREE) with strongly fractionated LREE to HREE, slight fractionation of HREE, and samples of the oldest magmatic episode having a distinctly stronger Eu anomaly. In primitive-mantle-normalized spidergrams (Fig. 6b), all the samples were enriched in Rb, Th, U, La, Ce, Nd and Hf, and depleted in Ba, Nb, Sr, P and Ti. Petrological and geochemical data suggest that whole-rock trace element characteristics for most samples were not markedly altered by regional alteration.

Sample LC-1 had an extremely high SiO_2 content (98.97 wt %), and the protolith was quartz porphyry, which was altered into siliceous rock under the action of later fluid and had a lower REE content. As observed petrographically, the characteristics of the whole rock display intense silicification. Sample LC-2 with 73.90 wt % SiO_2 content also exhibits relatively low ∑REE, which we interpret as resulting from strong alteration (Supplementary Table A.1, available online at https://doi.org/10.1017/S0016756822000863; Fig. 6). The whole-rock data of samples LC-1 and LC-2 do not represent primitive magmatic compositions.

4.c. O isotope composition of zircon grains

The zircon O isotope data are listed in Supplementary Table A.3 (available online at https://doi.org/10.1017/S0016756822000863). The weighted mean zircon $\delta^{18}O$ values of all samples ranged from 6 ‰ to 10 ‰. The zircon oxygen isotope compositions from the episode 1 granitic rocks (157.9–159.9 Ma) have a large range (from

https://doi.org/10.1017/S0016756822000863 Published online by Cambridge University Press

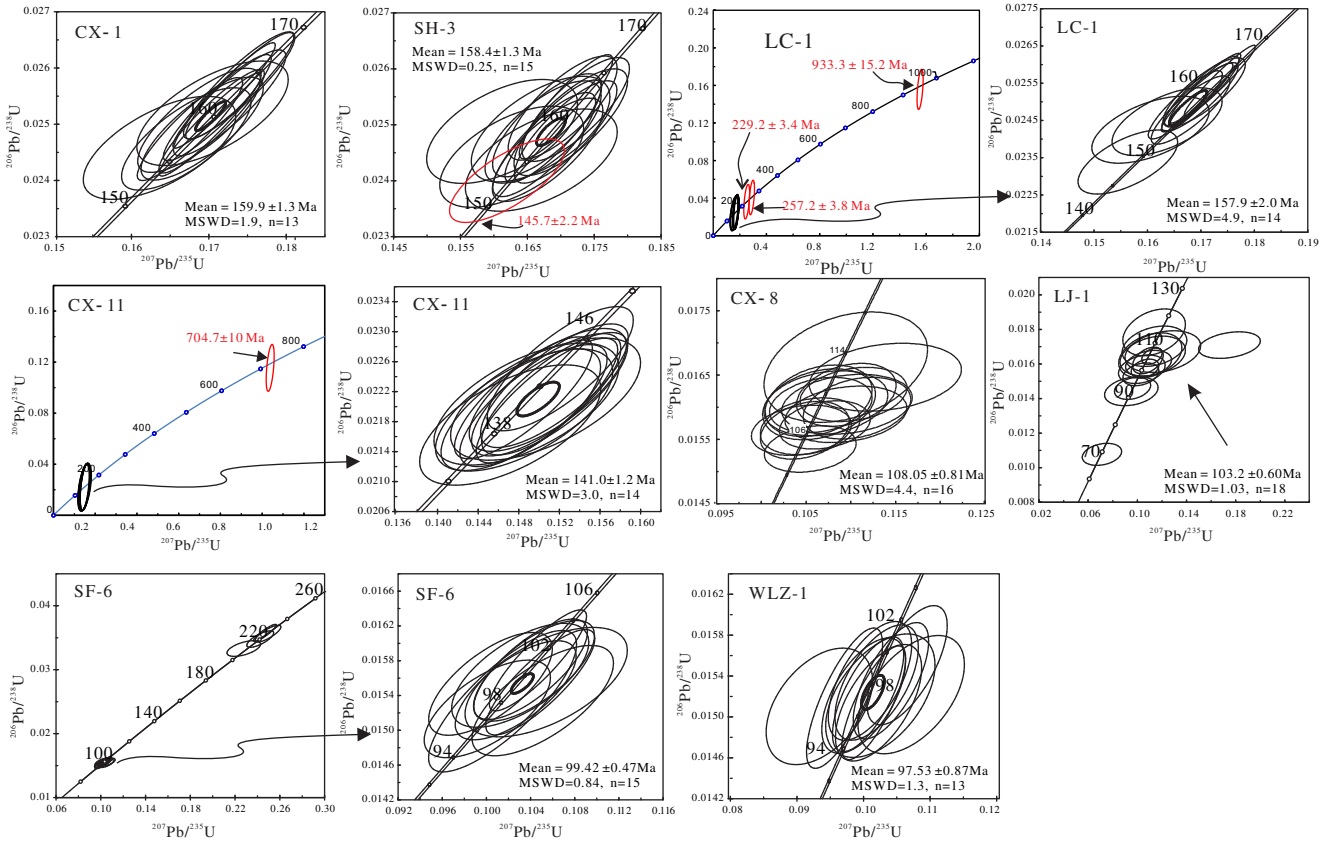

Fig. 4. (Colour online) U–Pb concordia plots illustrating the U–Pb ages of zircons from the Zijingshan area.

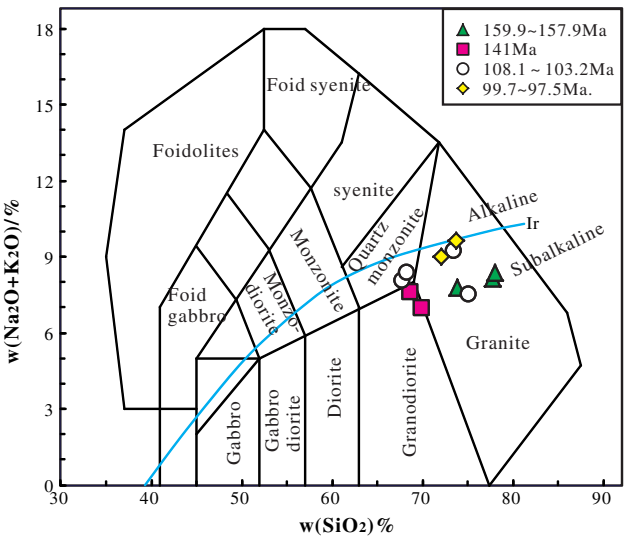

Fig. 5. (Colour online) SiO_2 vs $Na_2O + K_2O$(TAS) diagram. The Ir line marks the boundary between the alkaline rock series (top) and subalkaline rock series (bottom) (Middlemost, 1994).

6.49 to 11.96 ‰), with a mean value of 8.25 ± 0.30 ‰ (Fig. 7a). Zircon oxygen isotope compositions from episode 2 rocks (141 Ma) have largely homogeneous $\delta^{18}O$ (7.41–8.59 ‰). Episode 3 (108.1–103.2 Ma) and 4 (97.5–99.7 Ma) rocks have similar zircon oxygen isotope compositions, ranging from 6.28 to 7.78 ‰ and 6.64 to 8.56 ‰, respectively (Fig. 7a).

Additionally, five inherited zircon grains from LC-1 and SF-6 aged in the range 211.2–229.2 Ma show higher values of oxygen isotope compositions ($\delta^{18}O$ values from 7.26 to 10.73 ‰, with a mean value of 9.68 ‰; and one zircon grain (LC-1@5) aged at 257.2 ± 3.8 Ma shows the lowest $\delta^{18}O$ value ($\delta^{18}O = 5.51$ ‰) which was probably formed by hydrothermal alteration (Wei *et al.*, 2008).

4.d. Hf isotope composition of zircon grains

The analytical results are listed in Supplementary Table A.3 (available online at https://doi.org/10.1017/S0016756822000863) and shown in Figure 7b. The $\epsilon_{Hf}(t)$ values were calculated based on the U–Pb ages. Fifty-six spots for *in situ* Hf isotope analysis were determined on zircon grains from samples of episode 1 (157.9–159.9 Ma) and selected for *in situ* Hf isotope analysis, which yielded $\epsilon_{Hf}(t)$ values from 0.7 to −37.7 with an average value of −9.5, excluding two zircons which showed $\epsilon_{Hf}(t)$ values of −37.7 and −34.7, respectively. Twenty-eight analyses were performed for samples CX-10 and CX-11 in episode 2 (141.0 Ma), with $\epsilon_{Hf}(t)$ values varying from −22.6 to −7.3. Zircon grain CX-10@7 showed a more negative $\epsilon_{Hf}(t)$ value (−37.4). Twenty-eight analyses for episode 3 (108.1–103.2 Ma) yielded $\epsilon_{Hf}(t)$ values from −0.6 to −11.2, with an average value of −4.0. Thirty analyses for episode 4 (97.5–99.7 Ma) yielded $\epsilon_{Hf}(t)$ values from −2.8 to −11.4, with an average value of −6.6. Four spots from SF-6 with ages of 211–226 Ma yielded $\epsilon_{Hf}(t)$ values from −2.8 to −9.5.

https://doi.org/10.1017/S0016756822000863 Published online by Cambridge University Press

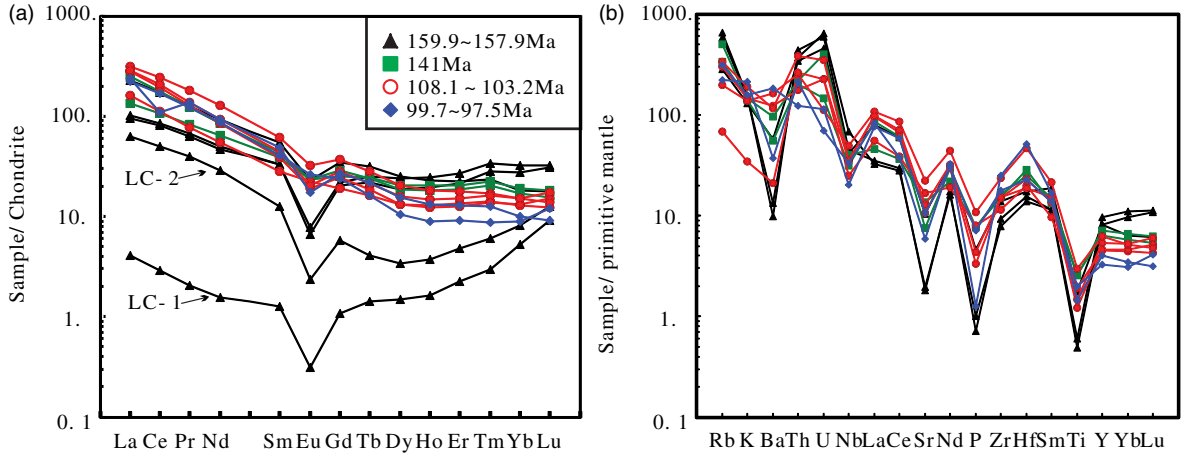

Fig. 6. (Colour online) Standardized rare earth element (a) and incompatible trace element (b; samples LC-1, LC-2 not plotted) diagrams. The values of chondrite and primitive mantle are from Sun & McDonough (1989).

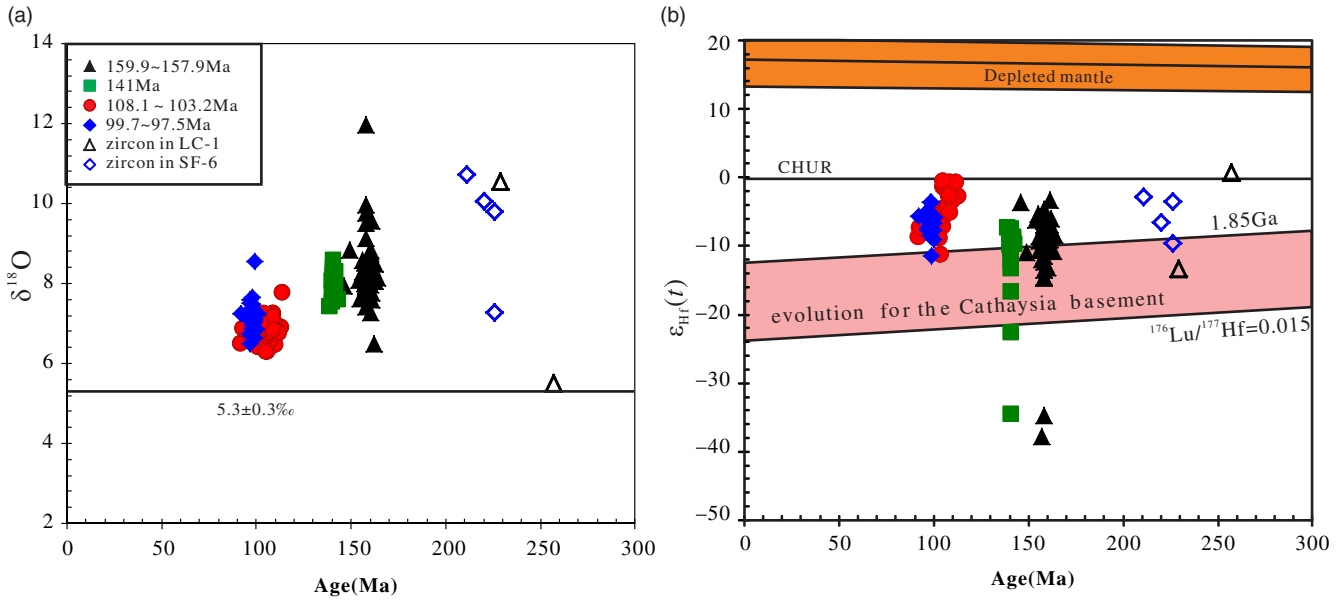

Fig. 7. (Colour online) (a) Zircon $\delta^{18}O$ vs age; mantle $\delta^{18}O$ value is according to Valley *et al.* (1998, 2005). (b) $\epsilon_{Hf}(t)$ vs age diagram, the ranges for depleted mantle after Griffin *et al.* (2002); Hf isotope evolution for Cathaysia crustal basement after Xu *et al.* (2007).

5. Discussion

In the Zijinshan area, magmatic zircon U–Pb ages showed that Mesozoic magmatism mainly occurred in the Jurassic and Cretaceous. Our SIMS U–Pb chronology data for the igneous rocks in this study can be divided into four episodes: episode 1: 157.9–159.9 Ma in the Late Jurassic (including CX-1, SH-3 and LC-1); episode 2: 141 Ma in the earliest Early Cretaceous (including CX-11); episode 3: 108.1–103.2 in the late Early Cretaceous (including CX-8 and LJ-1); and episode 4: 97.5–99.7 Ma in the earliest Late Cretaceous (including SF-6 and WLZ-1). The chronology data were consistent with the reported main age episodes in this area (e.g. Yu *et al.* 2013; Jiang *et al.* 2015; Li *et al.* 2016; Duan *et al.* 2017).

5.a. Influence of crust contamination and alteration

Sample LC-1 (granodiorites) of the first magmatic episode includes two Triassic zircons with ages of 229.2 Ma and 257.2 Ma. Sample SF-6 (monzonitic granite) of the fourth episode included four xenocrysts with ages ranging from 220.4 Ma to 226.4 Ma. This suggests that during the upwelling process the primitive magma suffered assimilation and contamination by Indosinian granitoids. Triassic-age magmatic rocks are also well developed around the Zijinshan area (Chen *et al.* 2011; Wang *et al.* 2013). Granitoid samples showed similar chondrite-normalized REE (Fig. 6a) and primitive-mantle-normalized incompatible patterns (Fig. 6b). The similarity of granites of different ages may represent similar source characteristics, except for LC-1 and LC-2 whose extremely high SiO_2 content indicates intense later alteration. Therefore, these two samples are ruled out in the following geochemical discussion. The freshest samples were selected in the field to ensure the least alteration, which is consistent with the results of the major element analysis that yielded loss-on-ignition values generally lower than 2 wt %. Zircon populations do not show obvious later alteration in light of both CL images and spot U–Pb analyses of

https://doi.org/10.1017/S0016756822000863 Published online by Cambridge University Press

zircon grains from Zijinshan granitoids. In summary, the granitoid samples were not makedly influenced by regional alteration and properly represent magmatic source characteristics.

5.b. Crust–mantle interactions for the late Jurassic and early Cretaceous granitoids

Although experimental petrology has shown that partial melting of ultramafic rocks in the mantle is unlikely to directly produce granitic magma (Johannes & Holtz, 1996), it is also widely accepted that mantle-derived magma can provide enough heat to melt the overlying crust formation and concurrently contribute to the crust-derived granitic melt in different proportions (Altherr *et al.* 2000). The change in the composition of the granitic melts predominantly depends on the ingredients of the lower crustal melt but is sometimes influenced by mantle-derived basaltic magma. Their chemical and isotopic compositions can be used to trace the nature of the magma sources in the lower crust (Wong *et al.* 2011).

Obvious negative Eu anomalies in chondrite-normalized REE (Fig. 6a) suggest that the fractional crystallization of plagioclase occurred in the source region. Zijinshan granitoids are enriched in LREEs and large-ion lithophile elements (LILEs; e.g. Rb, K, Th, U and Sr) and depleted in high-field-strength elements (HFSEs; e.g. Nb, Ta and Ti; Fig. 6b), implying a possible genetic relationship with arc-related magmatism. They are most likely derived from partial melting of the middle and lower crust and mixed mantle material which has been modified by subduction components. The increasing La/Yb value and decreasing content in HREE from episodes 1 to 4 (Fig. 6a) may reflect the deepening of the magmatic source or the involvement of more mantle-derived material with time.

Zircon has very low Lu/Hf ratios (commonly <0.002), resulting in non-radiogenic $^{176}Hf/^{177}Hf$ ratios. Therefore, the current zircon $^{176}Hf/^{177}Hf$ ratios can represent the initial ones that were inherited from the magma at the time of zircon crystallization (Wu *et al.* 2007).

Although it is speculated that the enriched Hf isotopic features of the granitoids may show crustal material affinities, the two-stage Hf model ages for most samples (T_{DM2} = 1.2–1.7 Ga) were markedly younger than those of the basement metamorphic rocks of the Cathaysia Block (>1.85 Ga; Xu *et al.* 2007). Most of the studied zircon $\epsilon_{Hf}(t)$ data for Zijinshan granitoids fell within the area between the depleted mantle and the Hf isotope evolution for the Cathaysia basement (Fig. 7b). It is thus inferred that the crust is not the single source of the magmas and some juvenile components from a depleted mantle source were also involved in generation of the studied granites; the granitoids in the Zijinshan region come from a mixture of mantle-derived components and crustal melts. Zircon U–Pb age determination indicates that the Late Yanshanian igneous rocks in SE China formed at four episodes of 141–130, 130–127, 123–118 Ma, and 110–86 Ma. These rocks show an oceanward-younging trend. *In situ* zircon Hf isotope analyses of igneous rocks show an increasing $\epsilon_{Hf}(t)$ trend, the entire sequences display typical isotopic features of magma mixing and there was a significant contribution of depleted asthenospheric mantle to the late-stage magmatism (He & Xu, 2012; Liu *et al.* 2014). Zircon $_{Hf}(t)$ values from episodes 1 (157.9–159.9 Ma) and 2 (141 Ma) granitoids were generally lower than those of zircons from episodes 3 (108.1–103.2 Ma) and 4 (97.5–99.7 Ma). Most of them were plotted in the region of Hf isotope evolution of the Cathaysia basement, indicating a higher proportion of reworked older crust. In contrast, the higher $\epsilon_{Hf}(t)$ values in episode 3 and 4 zircons imply that more mantle-derived magma contributed to the granitic magma. This suggests an increasing impact from a depleted asthenospheric mantle over time from the Late Jurassic to the Late Cretaceous.

Systematic *in situ* Hf and O isotope analyses of zircons indicate that mantle-derived materials play an important role in the generation of Zijinshan granites, which have variable Hf isotopic compositions that are different from the signature of magmas derived from a single source, indicating the involvement of mantle-derived magma. The Hf isotopic compositions of zircons from Zijinshan granitoids in episodes1 and 2 were generally highly variable, with the $\epsilon_{Hf}(t)$ values of most rocks ranging from 0.7 to −37.7 and T_{DM2} ages from 1.2 to 2.0 Ga. Large variations in zircon $\epsilon_{Hf}(t)$ values could be interpreted as indicating binary mixing between mantle-derived magma and evolved crustal components. The lower $\epsilon_{Hf}(t)$ values of zircon represent the isotopic signatures of felsic end-member melts that have undergone little or no mixing with mantle-derived components, whereas the higher $\epsilon_{Hf}(t)$ values of zircon indicate higher degrees of mixing (Li *et al.* 2014). The zircons in episode 3 (108.1−103.2 Ma) yield Hf T_{DM2} mainly in the range 1.2 to 1.7 Ga. This finding is consistent with the results of Jiang *et al.* (2013, 2015) and Liang *et al.* (2013), whose data collectively showed Hf T_{DM2} model ages of 1.0–1.6 Ga for zircons of Cretaceous granitoids in this area. However, Hf T_{DM2} ages in episode 4 are relatively older than those in episode 3, ranging from 1.4 to 1.8 Ga.

Oxygen isotopes have been extensively employed to trace magma sources and constrain the history of mantle-derived magma mixing with crustal materials. The mantle is a remarkably homogeneous oxygen isotope reservoir (Eiler, 2001), and igneous zircons in equilibrium with pristine mantle-derived melts have a narrow $\delta^{18}O$ (5.3 ± 0.3 ‰) (Valley, 2003; Cavosie *et al.* 2009). In contrast, magmas generated directly from or assimilated by crustal sources generally show higher $\delta^{18}O$ values (Eiler, 2001; Bindeman *et al.* 2005; Li *et al.* 2009*a*; Bindeman & Serebryakov, 2011; Spencer *et al.* 2017). Zircon O isotopic ratios noticeably higher than those of mantle zircon indicate that mantle-derived magma was considerably contaminated by crustal components during evolution, possibly due to the interaction of magma with Metasedimentary rocks that had experienced low-temperature or surface processes (with $\delta^{18}O > 10$ ‰; Valley *et al.* 2005). The rough correlation of zircon Hf and O isotopic ratios also suggests a degree of mixing of mantle- and crust-derived magmas in forming the granites.

The Zijinshan granitoids have lower zircon $\delta^{18}O_{Zrn}$ values (6.3–12 ‰; Fig. 7a) than those of typical crustal magmas (10–30 ‰; Valley *et al.* 2005), indicating the addition of mantle-derived materials or a pre-existing source region that was not influenced by surface processes (Cecil *et al.*2021). The zircon oxygen isotope values ($\delta^{18}O_{Zrn}$) of episodes 1 and 2 were mainly in the range 6.5–12.0 ‰, averaging 8.3 ‰ and 8.0 ‰, respectively. The $\delta^{18}O_{Zrn}$ values of episodes 3 and 4 were mainly in the range 6.3–8.6 ‰, averaging 6.8 ‰ and 7.2 ‰, respectively. As $\delta^{18}O_{Zrn}$ is insensitive to magmatic fractional crystallization (Valley, 2003), the higher-than-mantle $\delta^{18}O_{Zrn}$ values indicate a substantial crustal contribution. Magmatic rocks from episodes 3 and 4 with lower $\delta^{18}O_{Zrn}$ values reflect relatively lower crustal contributions compared to those found for episodes 1 and 2. In Fig. 7a, a significant decreasing trend of $\delta^{18}O_{Zrn}$ with age can be observed from the Late Jurassic to the Late Cretaceous, suggesting that periodically increasing mantle-derived magma contributed to crustal melts.

https://doi.org/10.1017/S0016756822000863 Published online by Cambridge University Press

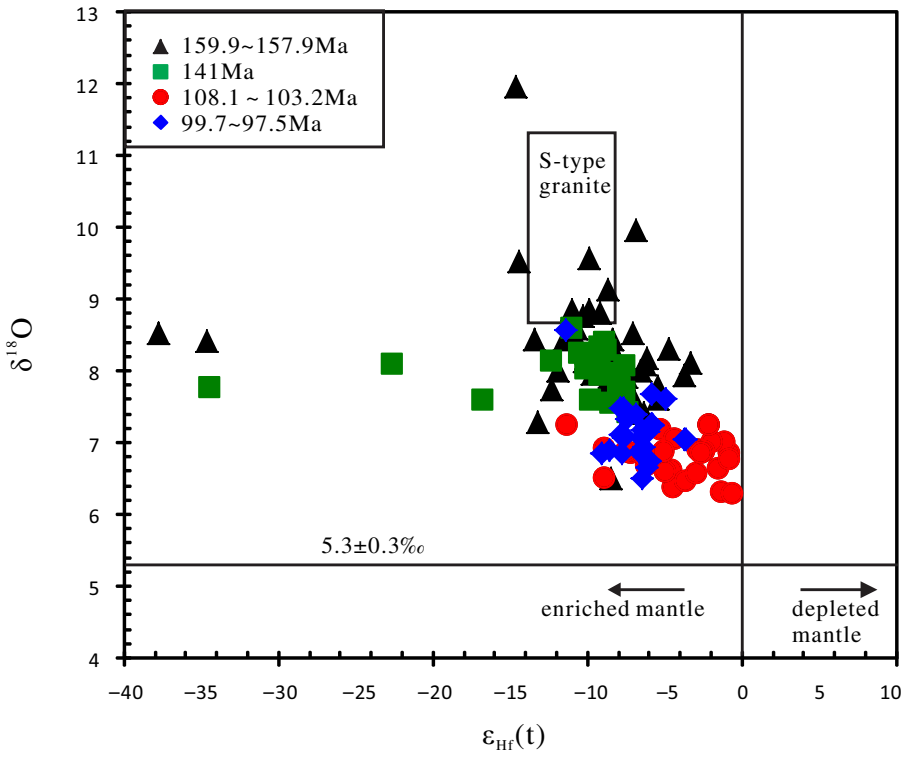

Fig. 8. (Colour online) $\delta^{18}O$ vs $\epsilon Hf(t)$ diagram. Zircon Hf–O isotope value for the S-type granite calculated from data for the Indosinian cordierite granite from Darongshan, Guangxi (Li *et al.* 2009*a*).

In the $\epsilon_{Hf}(t)$ vs $\delta^{18}O$ diagram (Fig. 8), the data exhibit an overall negative correlation. Zircon samples from all magmatic episodes show a gradual increase in $\epsilon_{Hf}(t)$ and a decrease in $\delta^{18}O$, consistent with the view of the progressive involvement of mantle-derived components. A lower-crustal source was likely the main magma origin area during the Late Jurassic, and the magmas from episodes 3 and 4 were likely more affected by a mantle-derived source. The higher $\delta^{18}O$ values of zircons in episodes 1 and 2, which are plotted in or near the S-type granite area, imply a sedimentary crustal source. The heterogeneous mixing of granitic magma remelted from sedimentary rocks with mantle-derived magma is probably the dominant formation process of these granites (Li *et al.* 2009*b*). The lower $\delta^{18}O$ values of zircons in episodes 3 and 4 indicate a significant mantle contribution to these magmas. This is consistent with new He and Ar isotope determinations from ore fluids from the Zijinshan Cu–Au and nearby Wuziqilong Cu deposits (dated 105 to 91 Ma), which show that volatility, heat and metals (at least part of them, if not all) may come directly from mantle-derived underplating of mafic magma (Wu *et al.* 2017). The relatively narrow range and low values of $\epsilon_{Hf}(t)$ and $\delta^{18}O$ in episode 3 and 4 granitic rocks of the Zijinshan region imply a greater continuous mantle influence (Figs. 7 and 9).

5.c. Geodynamic setting

The Zijinshan area is located to the east of the Nanling orogenic belt, which, in the late Mesozoic, was the transitional region from the collision and compression of the Indian and Eurasian plates to the subduction and expansion of the Palaeo-Pacific Ocean to the east of China (Zhang *et al.* 2001). The tectonic setting of SE China changed from a compressional subduction regime to an extensional regime during the Cretaceous at *c.* 110 Ma (He & Xu, 2012). Detailed studies of the Zijnshan igneous rocks suggest that Late Jurassic intrusions were emplaced in a compressional tectonic setting and Early Cretaceous granodiorite and volcanic rocks formed under an extension regime resulting from upwelling of the asthenosphere or a subduction-related tectonic setting (Zhang *et al.* 2001; Jiang *et al.* 2013). The transition from a compressional to an extensional tectonic environment in the SW Fujian region led to large-scale lithospheric thinning and magmatic activity in the region (Zhou *et al.* 2006; Qiu *et al.* 2008; Li *et al.* 2014; Wang *et al.* 2017).

In combination with whole-rock trace element data and zircon $\epsilon_{Hf}(t)$ and $\delta^{18}O$ features, we established a comprehensive model for the tectonic and magmatic evolution of Zijinshan granitic rocks. The Mesozoic (165–150 Ma) rock series and tectonic environment in SW Fujian indicate a Jurassic intracontinental overthrust environment with crust thickening (Mao *et al.* 2001). The heat generated by the strong thickening and shortening processes of the continental interior and possible additional heat input from mantle underplating caused crustal materials to begin to partially melt, and this resulted in the Late Jurassic granitic intrusions (Fig. 9). The transformation from regional compression to extension may have occurred at *c.* 135 Ma (Zhang *et al.* 2001; Mao *et al.* 2003). Under an extensional tectonic regime, crustal denudation and thinning contributed to the ascent and emplacement of magma (Mao *et al.* 2001). From the Late Jurassic to the Late Early Cretaceous period, the increasing $\epsilon_{Hf}(t)$ values, as well as the decreasing $\delta^{18}O$ values and T_{DM2} ages, suggest that the crust–mantle interaction gradually increased, corresponding to an enhanced extensional tectonic environment.

Subduction of the palaeo-Pacific plate has been widely accepted for interpreting Mesozoic tectono-magmatic activities in SE China. The extension of the lithospheric mantle coupled with upwelling of the asthenosphere resulted in large-scale, arc-affinity Cretaceous magmatism during the late Mesozoic period. Magmatism in the Zijinshan area could be grouped into early magmatic episodes (160–141 Ma) in a compressional environment and a late

https://doi.org/10.1017/S0016756822000863 Published online by Cambridge University Press

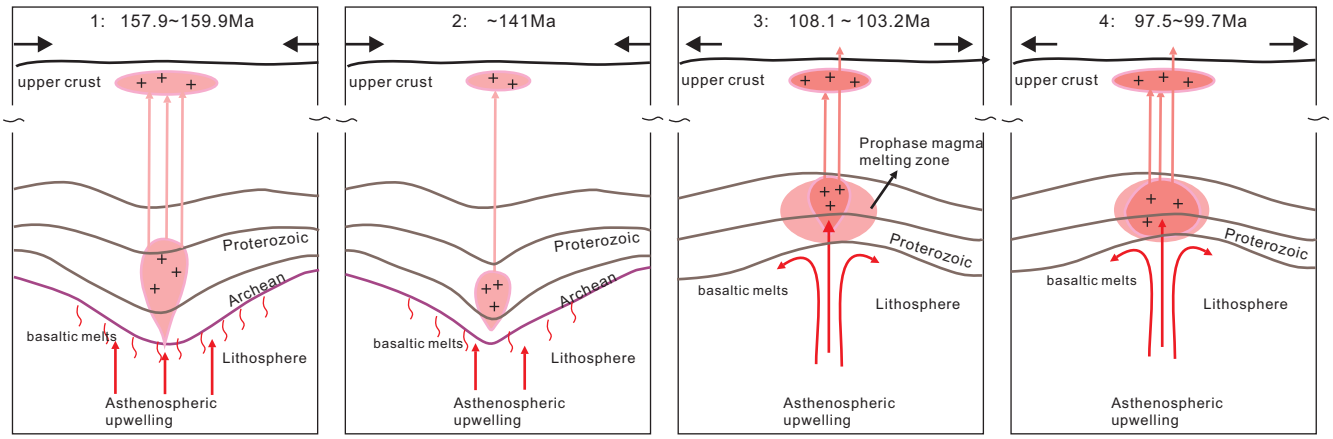

Fig. 9. (Colour online) Tectonic and magmatic evolution model for the Zijinshan granitic rocks.

magmatic episode (108–97 Ma) in an extensional environment, which were related to the forward and rollback subduction of the palaeo-Pacific plate, respectively. The granites in episodes 3 and 4 were emplaced at 108–97 Ma, corresponding to a period of rapid high-angle subduction of the palaeo-Pacific plate beneath SE China. In episodes 3 and 4, regional extension (~110 Ma) induced underplating of mantle-derived magmas and triggered the partial melting of the ancient basement rocks, producing felsic magmas. These crustal melts were then mixed with a small amount of mantle component to the granitic magma. During the same period, mantle-derived magma intruded between the lower crust and the lithospheric mantle, as manifested by the Mesozoic basic granulites in South China (Yu *et al.* 2002). Crust extension, thinning and mantle upwelling continued until 90 Ma (Mao *et al.* 2006). Crust–mantle interactions altered the composition of the original magma from the Late Jurassic to Early Cretaceous, which may explain the limited range in $\epsilon_{Hf}(t)$ and $\delta^{18}O$ values of episode 3 and 4 granitic rocks. The Zijinshan granitoids are the result of subduction-related magmatism due to a Cretaceous slab break-off and rollback of the subducting palaeo-Pacific plate (Mao *et al.* 2006; Yu *et al.* 2013; Li *et al.* 2014). During this geodynamic process, strong and rapid upwelling of the asthenospheric mantle occurred, causing regional extension of the overlying continental lithosphere and providing depleted mantle components for large-scale Late Jurassic to Late Cretaceous magmatism in the Zijinshan area.

6. Conclusions

(1) Our zircon SIMS U–Pb chronology data for the Zijinshan granitic rocks showed that the Zijinshan intrusive magmatism is divided into four episodes: episode 1: 157.9–159.9 Ma in the Late Jurassic; episode 2: 141 Ma in the earliest Early Cretaceous; episode 3: 108.1–103.2 Ma in the late Early Cretaceous; and episode 4: 97.5–99.7 Ma in the earliest Late Cretaceous.

(2) Crust–mantle interactions dictated the composition of the original magma. The increasing $\epsilon_{Hf}(t)$ values (−37.7 to −2.8), decreasing $\delta^{18}O$ values (12.0 to 6.3 ‰), increasing La/Yb values and decreasing trend in HREE from episodes 1 to 4 may indicate the increasing influence of mantle-derived material from the Late Jurassic to Late Cretaceous. The magma that intruded between 160 and 141 Ma (episodes 1 and 2) may have been derived mainly from melts of the lower crust. In contrast, the magma that intruded between 108 and 97 Ma (episodes 3 and 4) included more mantle-derived material.

(3) The tectonic and magmatic evolution of the Zijinshan granitic rocks in the late Mesozoic might have been caused by a structural change from the collision and compression of the Indian and Eurasian plates to the subduction and expansion of the Palaeo-Pacific Ocean to eastern China.

Supplementary material. To view supplementary material for this article, please visit https://doi.org/10.1017/S0016756822000863

Acknowledgements. This work was financially supported by the National Natural Science Foundation of China (No. 41873012, 41903007). The authors would like to thank the reviewers for helping in enhancing the paper.

References

Altherr R, Holl A, Hegner E, Langer C and Kreuzer H (2000) High-potassium, calc-alkaline I-type plutonism in the European Variscides: northern Vosges (France) and northern Schwarzwald (Germany). *Lithos* **50**, 51–73.

Belousova EA, Griffin WL, O'Reilly SY and Fishe N (2002) Igneous zircon: trace element compositions as indicators of source rock type. *Contributions to Mineralogy and Petrology* **143**, 602–22.

Bindeman IN, Eiler J M, Yogodzinski GM, Tatsumi Y, Stern CR and Grove TL (2005) Oxygen isotope evidence for slab melting in modern and ancient subduction zones. *Earth and Planetary Science Letters* **235**, 480–96.

Bindeman IN and Serebryakov NS (2011) Geology, petrology and O and H isotope geochemistry of remarkably O-18 depleted Paleoproterozoic rocks of the Belomorian Belt, Karelia, Russia, attributed to global glaciation 2.4 Ga. *Earth and Planetary Science Letters* **306**, 163–74.

Cavosie A J, Kita N T and Valley J W (2009) Primitive oxygen isotope ratio recorded in magmatic zircon from the Mid-Atlantic Ridge. *American Mineralogist* **94**, 926–34.

Cecil MR, Gehrels GE, Rusmore ME, Woodsworth GJ, Stowell HH, Yokelson I, Homan E, Kitajima K and Valley JW (2021) Mantle control on magmatic flare-ups in the southern Coast Mountains batholith, British Columbia. *Geosphere* **17**, 2027–41.

Chen CH, Hsieh PS, Lee CY and Zhou HW (2011) Two episodes of the Indosinian thermal event on the South China Block: constraints from LA-ICPMS U-Pb zircon and electron microprobe monazite ages of the Darongshan S-type granitic suite. *Gondwana Research* **19**, 1008–23.

Chen D, Deloule E, Cheng H, Xiao QK and Wu YB (2003) Preliminary study of oxygen isotope characteristics in the Dabie-Sulu metamorphic zircon microzone: ion probe in situ analysis. *Chinese Science Bulletin* **48**, 1732–9.

Chen JH (1999) The metallogenic mode of Zijinshan copper (gold) deposit. *Gold* **20**, 6–11 (in Chinese with English abstract).

Chi Z, Ni P, Pan JY, Li SN, Wang GG, Yang YL, Xue K and Liao JF (2020) Petrogenesis and tectonic setting of the Cretaceous volcanic-intrusive complex in the Zijinshan ore district, Southeast China: implications for different stages of mineralization. *Journal of Asian Earth Sciences* **192**, 104265.

Chu NC, Taylor RN, Chavagnac V, Nesbitt RW, Boella RM and Milton JA (2002) Hf isotope ratio analysis using multi-collector inductively coupled plasma mass spectrometry: an evaluation of isobaric interference corrections. *Journal of Analytical Atomic Spectrometry* **17**, 1567–74.

Duan G, Chen H, Hollings P, Duan G, Chen, HY, Hollings P, Qi JP, Xu C, Zhang S, Xiao B, Liu GY and Liu JM (2017) The Mesozoic magmatic sources and tectonic setting of the Zijinshan mineral field, South China: constraints from geochronology and geochemistry of igneous rocks in the Southeastern Ore Segment. *Ore Geology Reviews* **80**, 800–27.

Eiler JM. (2001) Oxygen isotope variations of basaltic lavas and upper mantle rocks. In *Reviews in Mineralogy and Geochemistry, vol. 43: Stable Isotope Geochemistry* (eds JW Valley and DR Cole), pp. 319–64. Washington, DC: Mineralogical Society of America.

Geng JZ, Li HK, Zhang J, Zhou HY and Li HM (2011) Zircon Hf isotope analysis by means of LA-MC-ICP-MS. *Geological Bulletin of China* **30**, 1508–13 (in Chinese with English abstract).

Griffin WL, Wang X, Jackson SE, Pearson NJ, O'Reilly, SY, Xu X and Zhou X (2002). Zircon chemistry and magma mixing, SE China: in-situ analysis of Hf isotopes, Tonglu and Pingtan igneous complexes. *Lithos* **61**, 237–69.

Griffin WL, Graham S, O'Reilly SY and Pearson NJ (2004) Lithosphere evolution beneath the Kaapvaal Craton: Re–Os systematics of sulfides in mantle-derived peridotites. *Chemical Geology* **208**, 89–118.

He ZY, and Xu XS (2012) Petrogenesis of the Late Yanshanian mantle-derived intrusions in southeastern China: response to the geodynamics of paleo-Pacific plate subduction. *Chemical Geology* **328**, 208–21.

He ZY, Xu XS and Niu YL (2010). Petrogenesis and tectonic significance of a Mesozoic granite-syenite-gabbro association from inland South China. *Lithos* **119**, 621–41.

Huang WT, Liang HY, Wu L, Wu J, Li J and Bao ZW (2018) Asynchronous formation of the adjacent epithermal Au-Cu and porphyry Cu-Mo deposits in the Zijinshan orefield, southeast China. Ore Geology Reviews 102, 351–67.

Jiang SH, Bagas L and Liang QL (2015) New insights into the petrogenesis of volcanic rocks in the Shanghang Basin in the Fujian Province, China. *Journal of Asian Earth Sciences* **105**, 48–67.

Jiang SH, Liang QL, Bagas L, Wang SH, Nie FJ and Liu YF (2013). Geodynamic setting of the Zijinshan porphyry–epithermal Cu–Au–Mo–Ag ore system, SW Fujian Province, China: constraints from the geochronology and geochemistry of the igneous rocks. *Ore Geology Reviews* **53**, 287–305.

Johannes W and Holtz F (1996) *Petrogenesis and Experimental Petrology of Granitic Rocks*. Minerals and Rocks 22. Berlin: Springer.

Li B, Zhao KD, Zhang Q, Xu YM and Zhu ZY (2015) Petrogenesis and geochemical characteristics of the Zijinshan granitic complex from Fujian Province, South China. *Acta Petrologica Sinica* **31**, 811–28 (in Chinese with English abstract).

Li D, Qiu X, Zhang W, Liu W and Yu B (2016) Zircon SHRIMP U-Pb and single mineral $^{40}Ar/^{39}Ar$ dating of granodiorite from the deep part of the Zijinshan Orefield in Fujian Province and its geological significance. *Geotectonica et Metallogenia* **40**, 783–97 (in Chinese with English abstract).

Li QL, Li X and Liu Y (2010) Precise U-Pb and Pb-Pb dating of Phanerozoic baddeleyite by SIMS with oxygen flooding technique. *Journal of Analytical Atomic Spectrometry* **25**, 1107–13.

Li XH, Li W, Wang X, Li QL, Liu Y and Tang GQ (2009a) Role of mantle-derived magma in genesis of early Yanshanian granites in the Nanling Range, South China: in situ zircon Hf–O isotopic constraints. *Science in China: Series D* **39**, 872–87.

Li XH, Li ZX, He B, Li WX, Li QL, Gao YY and Wang XC (2012) The Early Permian active continental margin and crustal growth of the Cathaysia Block: In situ U-Pb, Lu-Hf and O isotope analyses of detrital zircons. *Chemical Geology* **328**, 195–207.

Li XH, Liu Y, Li QL, Guo CH and Chamberlain KR (2009b) Precise determination of Phanerozoic zircon Pb/Pb age by multicollector SIMS without external standardization. *Geochemistry, Geophysics, Geosystems* **10**, 1–21.

Li XH, Long WG, Li QL, Liu Y, Zheng YF and Yang YH (2010) Penglai zircon megacrysts: a potential new working reference material for microbeam determination of Hf-O isotopes and U-Pb age. *Geostandards and Geoanalytical Research* **34**, 117–34.

Li XH, Tang GQ, Guo B, Yang YH, Hou KJ and Hu ZC (2013) Qinghu zircon: a working reference for microbeam analysis of U-Pb Age and Hf and O isotopes. *Chinese Science Bulletin* **58**, 1954–61.

Li Z, Qiu JS and Yang XM (2014) A review of the geochronology and geochemistry of Late Yanshanian (Cretaceous) plutons along the Fujian coastal area of southeastern China: implications for magma evolution related to slab break-off and rollback in the Cretaceous. *Earth-Science Reviews* **128**, 232–48.

Liang QL, Jiang SH, Wang SH, Li YF and Bai DM (2013) Petrogenesis of the Mesozoic magmatic rocks in Zijinshan area: constraints from zircon Hf isotope evidence. *Acta Petrologica et Mineralogica* **32**, 318–28 (in Chinese with English abstract).

Liu L, Xu X and Xia Y (2014) Cretaceous Pacific plate movement beneath SE China: evidence from episodic volcanism and related intrusions. *Tectonophysics* **614**, 170–84.

Mao JR, Chen R, Li JY, Ye HM and Zhao XL (2006) Geochronology and geochemical characteristics of Late Mesozoic granitic rocks from southwestern Fujian and their tectonic evolution. *Acta Petrologica Sinica* **22**, 1723–34 (in Chinese with English abstract).

Mao JR, Tao KY, Xie FG, Xu NZ and Chen SY (2001). Rock-forming and ore-forming processes and tectonic environments in Southwest Fujian. *Acta Petrologica et Mineralogica* **20**, 329–36 (in Chinese with English abstract).

Mao JW, Li XF, Zhang ZH, Wang YT and Hu HW (2003). Geology, distribution, types and tectonic settings of Mesozoic Epithermal gold deposits in East China. *Geological Journal of China Universities* **9**, 620–37 (in Chinese with English abstract).

Middlemost EAK (1994) Naming materials in the magma/igneous rock system. *Earth Science Reviews* **37**, 215–24.

Morag N, Avigad D, Gerdes A, Belousova E and Harlavan Y (2011) Crustal evolution and recycling in the northern Arabian-Nubian shield: new perspectives from zircon Lu–Hf and U–Pb systematics. *Precambrian Research* **186**, 101–16.

Qiu JS, Xiao E, Hu J, Xu XS, Jiang SY and Li Z (2008) Petrogenesis of highly fractionated I-type granites in the coastal area of northeastern Fujian Province: constraints from zircon U-Pb geochronology, geochemistry and Nd-Hf isotope. *Acta Petrologica Sinica* **24**, 2468–84 (in Chinese with English abstract).

Spencer CJ, Cavosie A J, Raub TD, Rollinson H and Evans NJ (2017) Evidence for melting mud in Earth's mantle from extreme oxygen isotope signatures in zircon. *Geology* **45**, 975–8.

Sun SS and McDonough W (1989) Chemical and isotopic systematics of oceanic basalts: implications for mantle composition and processes. In *Magmatism in the Ocean Basins* (eds AD Saunders and MJ Norry), pp. 313–45. Geological Society of London, Special Publication no. 42.

Valley JW. 2003. Oxygen isotopes in zircon. In *Reviews in Mineralogy and Geochemistry, vol. 53: Zircon* (eds JM Hanchar and WO Hoskin), pp. 343–85. Washington, DC: Mineralogical Society of America.

Valley JW, Kinny PD, Schulze DJ and Spicuzza MJ (1998) Zircon megacrysts from kimberlite: oxygen isotope variability among mantle melts. *Contributions to Mineralogy and Petrology* **133**, 1–11.

Valley JW, Lackey JS, Cavosie A J, Clechenko CC, Spicuzza MJ, Basei MAS, Bindeman IN, Ferreira VP, Sial AN, King EM, Peck WH, Sinha AK and Wei CS (2005). 4.4 billion years of crustal maturation: oxygen isotope ratios of magmatic zircon. *Contributions to Mineralogy and Petrology* **150**, 561–80.

Wang Q, Li JW, Jian P, Zhao ZH, Xiong XL and Bao ZW (2005). Alkaline syenites in eastern Cathaysia (South China): link to Permian–Triassic transtension. *Earth and Planetary Science Letters* **230**, 339–54.

Wang S, Zhang D, Wu G, Vatuva, A, Di Y and Yan P (2017). Late Paleozoic to Mesozoic extension in southwestern Fujian Province, South China: geochemical, geochronological and Hf isotopic constraints from basic-intermediate dykes. *Geoscience Frontiers* **8**, 529–40.

Wang YJ, Fan WM, Zhang GW and Zhang YH (2013) Phanerozoic tectonics of the South China block: key observations and controversies. *Gondwana Research* **23**, 1273–305.

https://doi.org/10.1017/S0016756822000863 Published online by Cambridge University Press

Wei CS, Zhao ZF and Spicuzza MJ (2008) Zircon oxygen isotopic constraint on the sources of late Mesozoic A-type granites in eastern China. *Chemical Geology* **250**, 1–15

Wiedenbeck M, Allé P, Corfu F, Griffin WL, Mmier M, Oberlif F, Vonquadt A, Roddick JC and Spiegel W (1995) Three natural zircon standards for U-Th-Pb, Lu-Hf, trace element and REE analyses. *Geostandards and Geoanalytical Research* **19**, 1–23.

Wong J, Min S, Xing G, Li XH, Zhao G, Wong, K and Wu FY (2011) Zircon U-Pb and Hf isotopic study of Mesozoic felsic rocks from Eastern Zhejiang, South China: geochemical contrast between the Yangtze and Cathaysia blocks. *Gondwana Research* **19**, 244–59.

Wu FY, Li XH, Zheng YY, Gao S (2007) Lu-Hf isotopic systematics and their applications in petrology. *Acta Petrologica Sinica* **2**, 185–220 (in Chinese with English abstract).

Wu FY, Yang YH, Xie LW, Yang JH and Xu P (2006) Hf isotopic compositions of the standard zircons and baddeleyites used in U–Pb geochronology. *Chemical Geology* **234**, 105–26.

Wu LY, Hu R Z, Li X F, Stuart FM, Jiang GH, Qi YQ and Zhu JJ (2017). Mantle volatiles and heat contributions in high sulfidation epithermal deposit from the Zijinshan Cu-Au-Mo-Ag orefield, Fujian Province, China: evidence from He and Ar isotopes. *Chemical Geology* **480**, 58–65.

Xu C, Chen HY, Huang WT, Qi JP, Duan G, Zhang LJ, Wu C, Zhang S and Zhong WB (2017) Mesozoic multiphase magmatism at the Xinan Cu–Mo ore deposit (Zijinshan Orefield): geodynamic setting and metallogenic implications. *Ore Geology Reviews* **88**, 768–90.

Xu XS, O'Reilly SY, Griffin WL, Wang XL, Pearson NJ and He ZY (2007) The crust of Cathaysia: age, assembly and reworking of two terranes. *Precambrian Research* **158**, 51–78.

Yu B, Pei RF, Qiu XP, Chen JH and Liu WY (2013) The evolution series of Mesozoic magmatic rocks in the Zijinshan Orefield, Fujian Province. *Acta Geoscientica Sinica* **34**, 437–46 (in Chinese with English abstract).

Yu J, Xu X and Zhou X (2002) Geochemistry study of basic granulite xenoliths along the coast of South China and composition of lower crust. *Science in China (Series D)* **32**, 383–93.

Zhang DQ, Li DX, Feng CY and Dong YJ (2001) The temporal and spatial framework of the Mesozoic magmatic system in Zijinshan area and its geological significance. *Acta Geoscientia Sinica* **22**, 403–8 (in Chinese with English abstract).

Zhang WH, Wang CZ, Li XM and Liu WY (2017) A primary discussion on magmatic evolution series in the Zijinshan area, Fujian Province: evidences from Zircon SIMS U-Pb ages and Hf, O isotopes. *Bulletin of Mineralogy, Petrology and Geochemistry* **36**, 98–111 (in Chinese with English abstract).

Zhao XY, Zhong H, Mao W, Bai ZJ and Xue K (2020) Molybdenite Re-Os dating and LA-ICP-MS trace element study of sulfide minerals from the Zijinshan high-sulfidation epithermal Cu-Au deposit, Fujian Province, China. *Ore Geology Reviews* **118**, 103363.

Zhong J, Chen YJ, Pirajno F, Chen J, Li J, Qi JP and Li N (2014) Geology, geochronology, fluid inclusion and H–O isotope geochemistry of the Luoboling porphyry Cu–Mo deposit, Zijinshan Orefield, Fujian Province, China. *Ore Geology Reviews* **57**, 61–77.

Zhou XM, Sun T, Shen WZ and Shu LS (2006) Petrogenesis of Mesozoic granitoids and volcanic rocks in South China: a response to tectonic evolution. *Episodes* **29**, 26–33.

https://doi.org/10.1017/S0016756822000863 Published online by Cambridge University Press